Journal of Power Sources 201 (2012) 322–331

Contents lists available at SciVerse ScienceDirect

Journal of Power Sources

journal homepage: www.elsevier.com/locate/jpowsour

Mathematical modeling of the LiAl/FeS_2 high temperature battery system

Tingting Yang, Long Cai, Ralph E. White*

Department of Chemical Engineering, University of South Carolina, Columbia, SC 29208, USA

ARTICLE INFO

Article history:
Received 23 September 2011
Accepted 2 November 2011
Available online 9 November 2011

Keywords:
Thermal battery
Precipitation
Volume change
Discharge capacity

ABSTRACT

A one dimensional mathematical model is presented for a high temperature lithium–aluminum, iron disulfide molten salt battery system. Multi-physics transport phenomena in the electrolyte, charge balances in the solid phases and electrolyte, complex multi-step electrochemical and chemical reactions in the electrodes are described in this model. The model includes the effects of precipitation salt on active area in the electrode and the discharge capacity. In addition the model also takes the change in volume of the active material into account during the electrochemical reactions by incorporating the change in porosity of the electrode and the change in dimension of the electrode. The model results are compared to the existing model in literature and available experimental data.

1. Introduction

With the oils crisis deepens, the demand of seeking alternative techniques for vehicle propulsion to reduce the dependence on the oil is growing. In addition, the requirement of the cheap energy sources has given impetus to the development of high-energy-density lithium batteries for various applications including electric vehicles, energy conversion and storage. To meet the need of the design of an electric vehicle battery, the system must have high specific energy density, long life and low cost. In addition, the safety, reliability, life and availability of materials also should be taken into consideration. As high power sources, high temperature batteries are served to provide power for off-peak storage devices and electric vehicle propulsion because of their main advantages such as long life, fast activation, rugged construction and high reliability [1–7]. Most high temperature batteries use lithium alloys (e.g. LiAl or Li(Si)) as anodes, metal-sulfides (e.g. FeS or FeS_2) as cathodes, and molten ionic conducting salts (e.g. LiCl–KCl, LiCl–LiBr–KBr, LiBr–KBr–LiF, LiCl–LiBr–LiF) as electrolytes. Among the various cathode materials, FeS_2 has its inherent advantages, such as well-predictable reactions, cheap cost and non-toxic properties [8]. However, it also has some disadvantages such as moderate thermal stability (about above 580 °C), significant solubility in molten salts and poor wetting properties by molten salts [8–10]. With the help of nanotechnology, the nanostructured FeS_2 has been prepared as a cathode material resulted in improved electrochemical performance [11]. In addition, FeS_2 electrode also leads the fashion of the thermal-sprayed electrode [12,13]. All these developments give an impulse to the LiAl/LiCl–KCl/FeS_2 high temperature system to have more applications due to its high open-circuit potential, high theoretical energy densities and inexpensive, non-toxic and green compounds which help this system to be safe.

In view of the promising future of the LiAl/LiCl–KCl/FeS_2 high temperature system, the investigation of the global function of the complex multi-step electrochemical, chemical reactions and the multi-physics phenomena occurred in the system is of vital importance. Mathematical modeling is an effective method in understanding the various complex processes involved in the system. The mathematical model for a LiAl/FeS battery system has been developed by Pollard and Newman [3]. Based on the mathematical model, Bernardi and Newman investigated the galvanostatic discharge behavior of lithium (alloy), iron disulfide cells [1]. However, these models only predicted the occurrence of the electrolyte precipitation salts based on the experimental results. In this work, the rate expression of the precipitation salts and its corresponding criteria have been presented, and the effects of the precipitation salts on the porosity and discharge capacity are also discussed. Furthermore, those models only considered the change in porosity of the electrode as the resulting effect due to the differences in molar volume of reactants and various products formed during the electrochemical reactions. The molar volume differences between the reactants and products actually also cause a change in dimension of the electrode in addition to the change in porosity. A mathematical model accounting for the porosity change during the discharge process has been developed for lithium ion battery [14] and lithium/thionyl chloride battery [15] systems. In both these models the changes in the active area due to porosity change as well as the dimension change of the electrode are incorporated. Unlike the lithium ion battery, the volume change or the expansion of the electrode is considerably large in the iron disulfide battery

* Corresponding author. Tel.: +1 803 777 3270; fax: +1 803 777 8265.
E-mail address: white@cec.sc.edu (R.E. White).

0378-7753/$ – see front matter © 2011 Published by Elsevier B.V.
doi:10.1016/j.jpowsour.2011.11.006

Nomenclature

a	specific area per unit electrode volume (cm^{-1})
a_0	initial specific area per unit electrode volume (cm^{-1})
A	cross-sectional area of the cell (cm^2)
C_p	specific heat ($J\,g^{-1}\,K^{-1}$)
D^{eff}	effective diffusion coefficient ($cm^2\,s^{-1}$)
F	Faraday's constant (96,487 C equiv.$^{-1}$)
h	heat transfer coefficient ($W\,m^{-2}\,K^{-1}$)
$i_{0,j}$	exchange current density ($A\,cm^{-2}$)
i_1	superficial current density in solid phase ($A\,cm^{-2}$)
i_2	superficial current density in electrolyte ($A\,cm^{-2}$)
I_{app}	applied current density ($A\,cm^{-2}$)
J_i	pore wall flux of species i ($mol\,cm^{-2}\,s^{-1}$)
k_p	precipitation rate constant ($cm^3\,mol^{-1}\,s^{-1}$)
L_n^0	initial negative electrode thickness (cm)
L_p^0	initial positive electrode thickness (cm)
L_p	the thickness of the positive electrode (cm)
L_s^0	initial separator thickness (cm)
L_T	total thickness of the cell (cm)
L_k	latent heat of fusion of salt k ($J\,mol^{-1}$)
m	mass of cell (kg)
n_j	number of electrons transferred in electrode reaction j
N	number of LiAl particles per unit electrode volume (cm^{-3})
r_β	radius of β-LiAl in LiAl pellet (cm)
r_α	radius of α-LiAl in LiAl pellet (cm)
R	universal gas constant ($8.3145\,J\,mol^{-1}\,K^{-1}$)
R_g	grid resistance ($\Omega\,cm^2$)
s_{ij}	stoichiometric coefficient of species i in electrode reaction j
S	swelling coefficient
t	time (s)
t_i^*	transference number of species i
T	absolute temperature (K)
T_{air}	temperature of surroundings (K)
T_0	initial temperature (K)
$U_{j,0}$	open-circuit potential for reaction j relative to a reference electrode (V)
u	local electrode displacement velocity ($cm\,s^{-1}$)
v^*	convective molar average velocity ($cm\,s^{-1}$)
V	cell voltage (V)
$\bar{V}_e$	molar volume of electrolyte ($cm^3\,mol^{-1}$)
$\bar{V}_k$	partial molar volume of salt k ($cm^3\,mol^{-1}$)
$\bar{V}_i$	partial molar volume of solid species i ($cm^3\,mol^{-1}$)
x_i	mole fraction of species i

Greek letters

$\alpha_{a,j}$	transfer coefficient in anodic direction
$\alpha_{c,j}$	transfer coefficient in cathodic direction
γ_A	activity coefficient of salt A
γ^{Li^+}	mean molar activity coefficient of lithium ion
ε	porosity
ε_n^0	initial porosity of the negative electrode
ε_s^0	initial porosity of the separator
ε_p^0	initial porosity of the positive electrode
ε_i	volume fraction of solid species i
$\varepsilon_{p,k}$	volume fraction of precipitation salt k
η	$\phi_1 - \phi_2$ (V)
η_j	overpotential of reaction j (V)
κ^{eff}	effective conductivity of the electrolyte ($S\,cm^{-1}$)
μ_A	chemical potential of salt A
σ^{eff}	effective conductivity of the solid phase ($S\,cm^{-1}$)
ϕ_1	solid phase potential (V)
ϕ_2	electrolyte potential (V)

Subscripts

app	applied
A	salt A, e.g., lithium chloride
B	salt B, e.g., potassium chloride
j	reaction j
k	precipitation of salt A or B
n	negative electrode
p	positive electrode
ref	reference electrode
s	separator

Superscript

eff	effective

system. Therefore the dimension/volume change has to be included for accurate prediction of the performance of the battery.

In this work, we have attempted to extend the model presented in Ref. [1] for a lithium–aluminum, iron disulfide high temperature battery system by including the expression of the rate of precipitation salts and the change in dimension of the electrode. The simulations are performed for battery performance at high temperature (450 °C). The model is validated by comparing with the experimental data available in the literature [16] and the existing model [1].

2. Model development

The model system consists of two porous electrodes: a positive electrode (FeS_2) and a negative reference electrode (LiAl) with a separator between them and a molten mixture of binary salt (LiCl–KCl) electrolyte throughout. Compared to Ref. [1], we did not consider the reservoir of electrolyte, because the emphasis of this model is to illustrate the precipitation effects and the volume change of the electrode which all occurred in the positive electrode, neglecting the reservoir of electrolyte do not alter the results of this model and can be considered as a valid assumption. For the given schematic of the cell in Fig. 1, during the discharge process lithium ions extract from the negative electrode, diffuse and migrate through the electrolyte and react with the active material in the positive electrode to form various intermediate products before a complete discharge. These processes can be described with the help of the porous electrode theory and transport equations derived for a binary salt mixture by Pollard and Newman [3,5].

Physical processes for a high temperature battery system include the diffusion, convection and migration of electrolyte species, local reaction rates, electrolyte precipitation rate, potential of the electrolyte and solid phase, changes in the porosity and electrolyte composition due to electrochemical reactions, energy balance and local electrode displacement velocities. The governing equations for a high temperature battery are summarized in the following sections and the modifications made to the original model [3] are explained.

2.1. Reactions in the cell

Initially, the negative electrode consists of β-lithium–aluminum particles which are assumed to be spherical and non-porous. As the discharge process proceeds, β-LiAl is oxidized to lithium

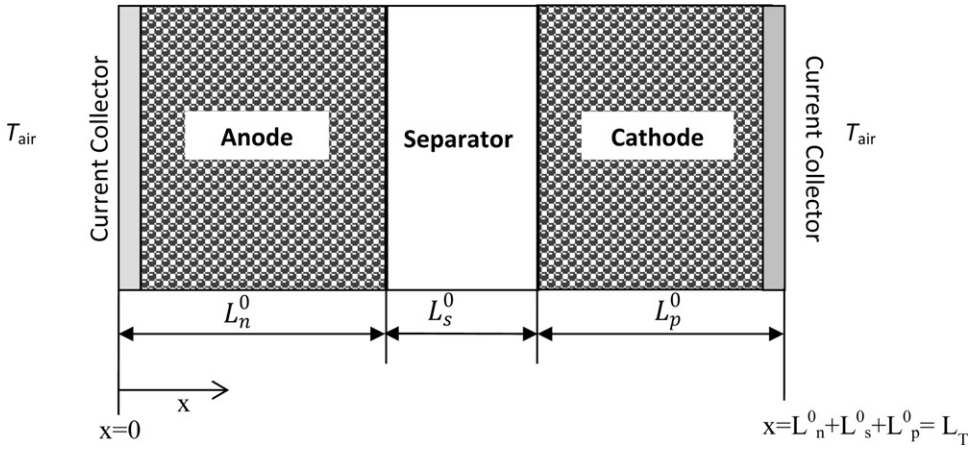

Fig. 1. Schematic of a LiAl/LiCl–KCl/FeS_2 cell sandwich consisting of porous cathode, anode and a separator in between.

ions and aluminum and leads to a layer of α-Al forming at the solid–electrolyte interface:

$$LiAl \rightarrow Li^+ + Al + e^- \quad (R1)$$

The discharge reactions occurred in the positive electrode have been investigated by many researchers. Among the various discharge mechanisms, the most accepted mechanism was advanced by Argonne National Laboratory, which follows four electron multistage reactions sequence [7]:

$$2FeS_2 + 3Li^+ + 3e^- \rightarrow Li_3Fe_2S_4\,(Z\text{-phase}) \quad (R2a)$$

$$Li_3Fe_2S_4 + 0.4Li^+ + 0.47e^- \rightarrow 1.58Li_{2.2}Fe_{0.8}S_2 + 0.84Fe_{0.875}S \quad (R2b)$$

$$Li_{2+x}Fe_{1-x}S_2 + Fe_{1-x}S \leftrightarrow Li_2FeS_2\,(X\text{-phase}) \quad (R2c)$$

$$Li_2FeS_2 + 2Li^+ + 2e^- \rightarrow 2Li_2S + Fe \quad (R2d)$$

Besides of the above electrochemical and chemical reactions, during the discharge process, a chemical precipitation reaction can also occur in the anode and cathode, respectively, as follows, in the melt saturated with LiCl–KCl mixtures:

$$Li^+ + Cl^- \leftrightarrows LiCl\,(s) \quad (R3)$$

$$K^+ + Cl^- \leftrightarrows KCl\,(s) \quad (R4)$$

2.2. Porous electrode model

The molten electrolyte and the solid phase are considered as a superimposed continuum according to the porous electrode theory. The material balances for the two binary salts with a common ion in a macro homogeneous medium are given by the following equations:

$$\frac{\partial(\varepsilon x_A/\bar{V}_e)}{\partial t} + \nabla\cdot\left(x_A g + (x_B t^*_{Li^+} - x_A t^*_{K^+})\frac{i_2}{F} - \frac{\varepsilon D^{eff}}{\bar{V}_e}\nabla x_A\right) = aJ_i \quad (1)$$

$$\frac{\partial(\varepsilon x_B/\bar{V}_e)}{\partial t} + \nabla\cdot\left(x_B g + (x_A t^*_{K^+} - x_B t^*_{Li^+})\frac{i_2}{F} - \frac{\varepsilon D^{eff}}{\bar{V}_e}\nabla x_B\right) = aJ_i \quad (2)$$

where

$$g = \frac{v^*}{\bar{V}_e} + (t^*_{Li^+} + t^*_{K^+})\frac{i_2}{F} \quad (3)$$

$\bar{V}_e$ is the molar volume of the electrolyte, x_A and x_B are mole fractions of the salt A (LiCl) and salt B (KCl), respectively, a is the specific area per unit electrode volume, v^* is the convective molar average velocity and the transferences number are $t^*_{Li^+} = x_A/2$ and $t^*_{K^+} = x_B/2$. The convection shown in Eq. (3) is considered negligible compared to the change in molar volume of the electrolyte solution, $\Delta v^*/\Delta\bar{V}_e \ll 1$, which has been shown as a valid assumption for this system [4].

By neglecting the double-layer charging and applying a modified Faraday's law [3], the mass transfer rate of species i, aj_i, between the electrolyte and the solid phase is given by:

$$aj_i = -\sum_j \frac{s_{ij} a i_j}{n_j F} - \frac{1}{\bar{V}_k}\frac{\partial\varepsilon_{p,k}}{\partial t} \quad (4)$$

where i represents the species of Li or K, j represents reaction (R1) for the negative electrode and indicates individual reaction (R2a)–(R2c) or (R2d) for the positive electrode, k is the precipitation of salt A (LiCl) or B (KCl), s_{ij} is the stoichiometric coefficient of species i for reaction j and n_j is the number of the electrons for reaction j. The physical meaning of last term on the right side of Eq. (4) is the removal rate of species i from the electrolyte due to the precipitation of salt k, and it is given by [17]:

$$\frac{\partial\varepsilon_{p,k}}{\partial t} = k_p \times \frac{\bar{V}_k}{\bar{V}_e^2}(x_k - (x_A)_{k,sat}) \quad (5)$$

where k_p is the precipitation rate constant, $\bar{V}_k$ is the molar volume of salt k, $(x_A)_{k,sat}$ is the saturation composition. When the mole fraction of salt k is larger than the saturation composition, precipitation reaction occurs.

Because $x_B = 1 - x_A$, combining Eqs. (1), (2) and (5) yields the following equation:

$$\frac{\partial\varepsilon x_A/\bar{V}_e}{\partial t} = \nabla\cdot\left(-\frac{x_A i_2}{2F} + \frac{\varepsilon D^{eff}}{\bar{V}_e}\nabla x_A\right) - \sum_j \frac{s_{Li^+,j} a i_j}{n_j F} - \frac{1}{\bar{V}_{LiCl}}\frac{\partial\varepsilon_{p,LiCl}}{\partial t} \quad (6)$$

The superficial current density in the electrolyte, i_2, is given by the following expression:

$$i_2 = \kappa^{eff}\left(\nabla\phi_2 + \frac{1}{F}\left[\left(\frac{s_{Li^+,j}}{n_j} + x_A\right)\frac{1}{x_B} - \frac{s_{Cl^+,j}, x_A}{n_j x_B}\right]\nabla\mu_A\right) \quad (7)$$

where κ^{eff} is the effective conductivity of the electrolyte, ϕ_2 is the electrolyte potential and μ_A is the chemical potential of LiCl.

The current density in the solid phase is given by

$$i_1 = -\sigma^{eff}\nabla\phi_1 \quad (8)$$

where σ^{eff} is the effective solid conductivity and ϕ_1 is the solid phase potential.

Table 1
Coefficients for the open-circuit potential of the FeS_2 electrode.

Reaction	a_j (V)	b_j ($\times 10^3$ V K^{-1})
(R2a)	1.4251	0.4785
(R2b)	1.208771	0.65142
(R2c) (in Eq. (14))	1.3389	0.0133
(R2d)	1.43211	−0.147

A charge balance for the current and the electrochemical reaction yields the following equation:

$$\nabla \cdot i_1 = -\nabla \cdot i_2 = -ai_j \tag{9}$$

where ai_j is the local transfer current per unit volume of the electrode due to reaction j and can be expressed by the polarization equation:

$$ai_j = ai_{0,j}\left[\exp\left(\frac{\alpha_{a,j}F}{Rt}\eta_j\right) - \exp\left(\frac{\alpha_{c,j}F}{Rt}\eta_j\right)\right] \tag{10}$$

where η_j is the local surface overpotential, $\eta_j = \phi_1 - \phi_2 - U_j$, and a is the specific area per unit electrode volume which is assumed here to be proportional to volume fraction of solid phase i, ε_i

$$a = a_0\varepsilon_i \tag{11}$$

where a_0 is the initial specific area per unit electrode volume.

The exchange current density for reaction j, $a_{0,j}$, can be written as

$$i_{0,j} = i_{0,j,ref}\left(\frac{x_A}{x_{A,ref}}\right)\gamma_i \tag{12}$$

where $\gamma_i = 0.5$ (assumed value) and $x_{A,ref}$ is equal to the initial electrolyte composition.

The theoretical open-circuit potential for reactions (R2a), (R2b) and (R2d) depends on the temperature and is given by:

$$U_j = a_j + b_jT \tag{13}$$

The values for the coefficients a_j and b_j are shown in Table 1 [1].

The open-circuit potential for reaction (R2c) is given by:

$$U_{R2c} = U_{R2b} + \frac{(a_c - a_{R2b}) + T(b_c - b_{R2b})}{1 - ((2.2(4x_0' - 2)/(2x_0' - 0.8)) - 3)}\left[\frac{q_{R2c}2\bar{V}_{FeS_2}}{\varepsilon^0_{FeS_2}F}\right] \tag{14}$$

where x_0' depends on the following linear variations of temperature, q_{R2c} is the number of coulombs of charge passed for reaction (R2c) per unit volume of the positive electrode:

$$x_0' = -9.240 \times 10^{-5}T + 0.91658 \tag{15}$$

$$q_{R2c} = \int_0^t ai_{R2c}\ dt \tag{16}$$

All electrode reaction potentials shown in Eq. (13) are given relative to a two-phase (α–β) LiAl reference electrode.

According to the analysis in Ref. [3], at the fully charged state in the negative electrode, the negative electrode consists of spherical, nonporous structured β-LiAl particles. When the discharge process starts, the reaction (R1) first occurs on the outward region of the particle which results in the establishment of a layer of α-LiAl whose thickness gradually grows at the cost of β-LiAl. The Bulter–Volmer equation shown in Eq. (10) is modified by considering the diffusion overpotential for the mass transport of lithium ions across the α-phase to the solid–electrolyte interface and is given by [5]:

$$ai_j = \nabla \cdot i_2 = \frac{\exp((\alpha_aF/RT)\eta) - \exp((-\alpha_aF/RT)\eta)}{(1/(4\pi Nr_\alpha^2 i_{0,ref}(x_A/x_{A,ref})\gamma^{Li^+})) + ((\exp(\alpha_aF/RT)\eta)/(\nabla \cdot i_2)_{lim})} \tag{17}$$

where γ^{Li^+} is the mean molar activity coefficient of lithium ions and $(\nabla \cdot i_2)_{lim}$ is the diffusion-limited transfer current and can be expressed by:

$$(\nabla \cdot i_2)_{lim} = \frac{4\pi NFD_\alpha(x^\alpha_{Li})_{sat}}{(1 - \bar{x}^\alpha_{Li})((1/r_\alpha) - (1/r_\beta))} \tag{18}$$

where $(x^\alpha_{Li})_{sat}$ is the saturated mole fraction of lithium in the α-phase, $\bar{x}^\alpha_{Li}$ is the average mole fraction of lithium in the α-phase; r_α and r_β are the radius of the α-phase and β-phase in the negative electrode, whose expressions are given in Ref. [5].

2.3. Volume and porosity changes in solid phase

The volume change effects during discharge process manifest in two forms: change in porosity and change in electrode dimensions. This is because when the chemical and electrochemical reactions occur, the products formed on the surface of the electrode particles occupy a part of the pore volume and push the electrode particles away from each other.

The change in porosity of the electrode during the operation of battery occurs due to the differences in molar volumes of the reactants and the products in the chemical and electrochemical reactions. The volume fraction of solid phase i is given by:

$$\frac{\partial\varepsilon_i}{\partial t} = \frac{s_{ij}\bar{V}_i}{n_jF}ai_j \tag{19}$$

where ε_i and $\bar{V}_i$ are the volume fraction and molar volume of the solid species i, respectively.

The appreciable molar volume differences between the reactant and various products formed at the cathode do not only lead to the change of porosity, but also result in the cathode swelling. The change in electrode dimension is governed by the local electrode displacement velocity, u, which is given by the following equation [18]:

$$\nabla \cdot u = S\sum_j \frac{-s_{ij}\bar{V}_i}{n_jF(1-\varepsilon)}ai_j \tag{20}$$

where ε is the porosity of the cathode, S is the swelling coefficient, an empirical quantity and can be estimated for the particular battery system based on the design of the electrode and operating conditions as demonstrated in Ref. [18]. Eq. (20) shows the relationship between the local electrode displacement velocity and the porosity.

The thickness of the positive electrode L_p is calculated as follows:

$$\frac{\partial L_p}{\partial t} = u|_{x=L_T} \tag{21}$$

2.4. Thermal effects

The temperature of the battery changes during the discharge process due to reversible heat of the reaction, heat losses to the surrounding atmosphere, joule heating and dissipation of latent heat because of the precipitation reaction.

The energy balance of the cell is given by:

$$\frac{mC_p}{A}\frac{\partial T}{\partial t} = \left(\sum_j \left(U_{j,0} - T_0\frac{\partial U_j}{\partial T}\right)\right) I_{app} - VI_{app} - h(T - T_{air}) + \sum_k \frac{L_k}{\bar{V}_k}\int_0^{L_T} \frac{\partial \varepsilon_{p,k}}{\partial t}\, dx \quad (22)$$

where m is the mass of the cell, C_p is the specific heat, A is the cross-sectional area of the cell, $U_{j,0}$ is the open circuit potential at 450 °C for reaction j, h is the heat transfer coefficient and L_k is the latent heat of fusion of salt k.

Mole fraction of salt A (x_A), solid potential (ϕ_1), electrolyte potential (ϕ_2), volume fraction of precipitation salt k ($\varepsilon_{p,k}$), volume fraction of solid species i (ε_i), local electrode displacement velocity (u), the thickness of the cathode (L_p) and temperature (T) can be solved as the dependent variables. The governing equations described by Eqs. (5)–(8) and (19)–(22) along with the corresponding initial conditions and boundary conditions described in the following section.

2.5. Boundary and initial conditions

Fig. 1 shows a schematic of a high temperature cell, which consists of four boundaries and three regions. At the current collector/electrode boundaries, the flux of the species in the electrolyte is set to zero

$$\text{At } x = 0 \quad \text{and} \quad x = L_T, \quad \nabla x_A = 0 \quad (23)$$

The solid phase potential is equal to zero at the negative current collector and the solid phase current density is set equal to the applied current density at the positive current collector

$$\begin{aligned} &\text{At } x = 0, \quad \phi_1 = 0 \\ &\text{At } x = L_T, \quad i_1 = I_{app} \end{aligned} \quad (24)$$

The electrolyte current density is set equal to zero at the current collector/electrode boundaries

$$\text{At } x = 0 \quad \text{and} \quad x = L_T, \quad i_2 = 0 \quad (25)$$

The local electrode displacement velocity of the electrode is set to be zero at the separator/positive electrode boundary

$$u|_{x=L_n+L_s} = 0 \quad (26)$$

There is no electrochemical reaction occurred in the separator. The material balance of electrolyte composition in the separator is the same as that in the cathode and anode except that the porosity is a constant in the separator. At the interior boundaries all the fluxes are assumed to be continuous.

The initial values are specified as follows:

$$\text{At } t = 0, \quad m = n \text{ (negative electrode)}, \quad s \text{ (separator)}, \quad \text{or } p \text{ (positive elecrode)}$$

$$\begin{cases} x_A = x_A^0 \\ \varepsilon_m = \varepsilon_m^0 \\ u = 0 \\ T = T_0 \\ L_p = L_p^0 \end{cases} \quad (27)$$

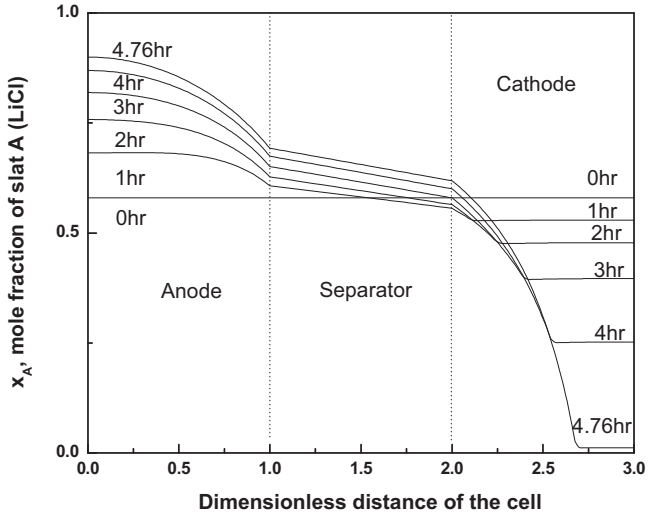

Fig. 2. Position dependence of mole fraction of LiCl at different discharge times (I_{app} = 41.6 mA cm^{-2}).

3. Solution procedure

The numerical simulations were carried out in COMSOL Multiphysics 4.1 [19] by using the finite element method to discretize the governing equations.

3.1. Discretization scheme

Each model region (negative electrode, separator and positive electrode) is discretized along the x coordinate. The variables solved for in all three regions are: {x_A, ϕ_2 and T}; ϕ_1 is solved for in the positive and negative electrode. Volume fraction of the solid phase (ε_i), volume fraction of precipitation salt k ($\varepsilon_{p,k}$) and the local electrode displacement velocity (u) are solved for only in the positive electrode. To evaluate the dimension change of the electrode, the thickness of the anode, separator, and cathode are converted to the form of dimensionless, respectively. Because the dimension change is only occurred in the cathode in this work, the thickness of the cathode (L_p), as a variable is calculated based on velocity (u) at the current collector/positive electrode interface at each time step.

3.2. Parameters

The design parameters, other parameters and their values used in the simulation are shown in Table 2. The physical properties of the electrolyte and the solid phases are listed in Appendix A. To point it out, the swelling coefficient S is a parameter that determines the relative magnitude of the porosity change and the electrode dimension change. The range of S is from 0 to 1, we choose S = 0.5. The number of elements in the negative electrode and separator is 30; the number of elements in the positive electrode is 96 with 1.3 element growth rate. The relative tolerance is 1e−6 and the absolute tolerance is 1e−4.

4. Results and discussion

4.1. Electrolyte composition

Fig. 2 shows the electrolyte composition profiles across the cell sandwich for several times with a constant discharge current density of 41.6 mA cm^{-2}. A distinct electrolyte composition profile is established on the base of dimensionless thickness. Before the discharge process starts, the mole fraction of salt LiCl remains as

Table 2
Parameters used in the simulation.

Parameter	Cathode	Anode	Separator	Reference
Electrode parameters				
L_m^0 (cm)	0.2146	0.4048	0.16	[1]
ε_m^0	0.75	0.39	0.75	[1]

Parameter	Cathode	Anode	Reference
Kinetics parameters			
$\alpha_{a,j} = \alpha_{c,j}$	1	0.5	[3]
n_j	2.0	1.0	[3]
$S_{Li^+,j}$	−2.0	1.0	[3]
$S_{Cl^-,j}$	0.0	0.0	[3]
$(x_A)_{ref}$	0.68	0.68	[1]
i_0 (A cm^{-2})		2.8	[3]
$(a_0 i_0)_j$ (A cm^{-3})	2.0e3		[3]
D_α (cm^2 s^{-1})		4.0e−10	[3]
$\bar{x}_{Li}^{\alpha}$		0.05	[3]
γ^{Li^+}		0.5	[3]
Other parameters			
σ_{FeS_2} ($(\Omega\,cm^{-1})^{-1}$)		100	[1]
$\sigma_{Li_3Fe_2S_4(Z\text{-phase})}$ ($(\Omega\,cm^{-1})^{-1}$)		0.2	[1]
$\sigma_{Li_2FeS_4(X\text{-phase})}$ ($(\Omega\,cm^{-1})^{-1}$)		5.1	[1]
σ_{Fe} ($\Omega\,cm^{-1})^{-1}$		8.3e4	[1]
σ_{Li_2S} ($\Omega\,cm^{-1})^{-1}$		0	[1]
$\bar{V}_{FeS_2}$ (cm^3 mol^{-1})		23.93	[1]
$\bar{V}_{Z\text{-phase}}$ (cm^3 mol^{-1})		99.17	[1]
$\bar{V}_{X\text{-phase}}$ (cm^3 mol^{-1})		49.82	[1]
$\bar{V}_{Fe}$ (cm^3 mol^{-1})		18.49	[1]
$\bar{V}_{Li_2S}$ (cm^3 mol^{-1})		28.062	[1]
$s_{FeS_2,3a}$		−4/3	[1]
$s_{Z\text{-phase},3a}$		2/3	[1]
$s_{Z\text{-phase},3a(3c)}$		−2	[1]
$s_{X\text{-phase},3b(3c)}$		4	[1]
$s_{X\text{-phase},3d}$		−1	[1]
$s_{Li_2S,3d}$		2	[1]
$s_{Fe,3d}$		1	[1]
$\bar{V}_{KCl}$ (cm^3 mol^{-1})		20.5	[3]
L_{KCl} (J mol^{-1})		25,500	[5]
N (1 cm^{-3})		0.5e7	[5]
mC_p/A (kJ kg^{-1} K^{-1})		1.89	[5]
F (C mol^{-1})		96,487	
R (J mol^{-1} K^{-1})		8.3143	
h (W m^{-2} K^{-1})		8.25e−2	[3]
T_{air} (K)		298.15	
R_g (Ω cm^2)		1.55	[3]
S		0.5	Assumed value
k_p (cm^3 mol^{-1} s^{-1})		0.001	Assumed value

a constant that is the initial condition 0.58. When the discharge begins, lithium ions are introduced into the electrolyte from the negative electrode and transport across the separator to the positive electrode, where they can react with FeS_2 and finally form Fe and Li_2S. Fig. 2 shows that as the discharge proceeding, the mole fraction of lithium ions increases in the anode due to reaction (R1). All the discharge reactions occurred in the cathode consume lithium ions, which deeply decrease the amount of lithium ions. At the end of the discharge, the mole fraction of lithium ions is almost down to zero. A constant composition gradient is observed across the separator due to the constant flux of lithium ions in the separator.

The details of the composition variations can be attributed to the combined effects of diffusion, migration, electrochemical reactions and phase transitions. In the electrodes, a small change of the local porosity may intensify the variations of the electrolyte compositions.

4.2. Volume fractions of solid phases distribution

According to the discharge mechanism proposed by ANL, there are four intermediate phases, $Li_3Fe_2S_4$ (Z-phase), $Li_{2+x}Fe_{1-x}S_2$, $Fe_{1-x'}S$ and Li_2FeS_2 (X-phase). For the $Li_{2+x}Fe_{1-x}S_2$ and $Fe_{1-x'}S$ compounds, we do not have molar volume data because they are the functions of the composition variable x. We simplify the phase transitions as Ref. [1] did. Reactions (R2b) and (R2c) can be combined into one reaction

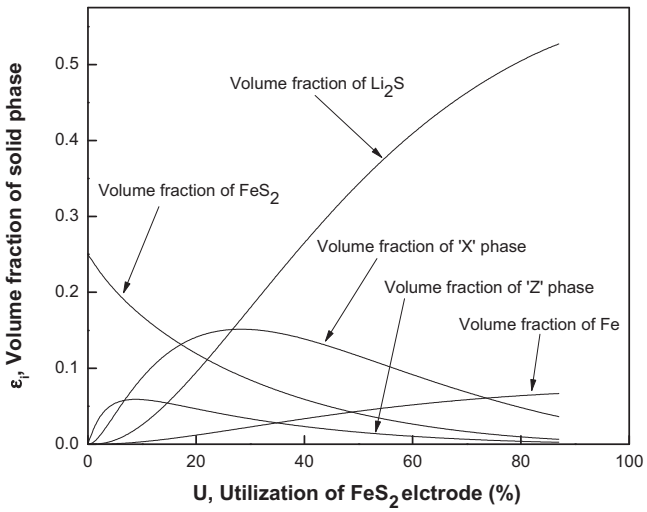

Fig. 3. Volume fractions of solid phases on the interface between the cathode and the current collector as a function of utilization of FeS_2 electrode (I_{app} = 41.6 mA cm^{-2}).

$$Li_3Fe_2S_4\,(Z\text{-phase}) + Li^+ + e^- \rightarrow 2Li_2FeS_2\,(X\text{-phase}) \quad (R5)$$

Based on this approximation, the intermediate phases are $Li_3Fe_2S_4$ (Z-phase) and Li_2FeS_2 (X-phase). We calculate the volume fractions of the solid phases in the positive electrode according to three reactions (R2a), (R5) and (R2d). This simplification is accurate because reactions (R2b) and (R2c) are the intermediate reactions and can reach the completion at the end of the discharge process. Fig. 3 shows the volume fractions of the solid phases in the positive electrode. The utilization is defined by the following expression which can be considered as a dimensionless time during the discharge process:

$$\%\ \text{utilization of } FeS_2 = \frac{100 I_{app} t \bar{V}_{FeS_2}}{L_p^0 \varepsilon_{FeS_2}^0 4F} \quad (28)$$

where $\bar{V}_{FeS_2}$ is the molar volume of FeS_2, L_p^0 is the initial thickness of the positive electrode, $\varepsilon_{FeS_2}^0$ is the initial porosity of the positive electrode and I_{app} is the applied current density.

The species considered to exist during the discharge process in the positive electrode include the initial active material: FeS_2, the intermediate products: Z-phase and X-phase and the final products: Li_2S and Fe. Fig. 3 presents the volume fractions of solid phases on the interface between the cathode and the current collector as a function of utilization of FeS_2 electrode. The simulation results are under the condition of 68% (mole ratio) lithium chloride in the electrolyte. The volume fraction of the FeS_2 decreases with the utilization of FeS_2 during the discharge process. The volume fraction of Z-phase first increases at about 9% utilization and then decreases. The reduction of the volume fraction of Z-phase indicates the rate of reaction (R2a) is slower than the rate of reaction (R2b). When the volume fraction of Z-phase falls to a small and stable value, it means that the reaction (R2b) approaches to the completion. The volume fraction of X-phase has the similar trend as the volume fraction of Z-phase, but left behind, which confirms that the sequence of the reactions occurred in the positive electrode is correct. For the final products Fe and Li_2S, their volume fractions always increase as the discharge process proceeding. Compared to the volume fraction of Fe, the amount of the volume fraction of Li_2S is much larger. This is

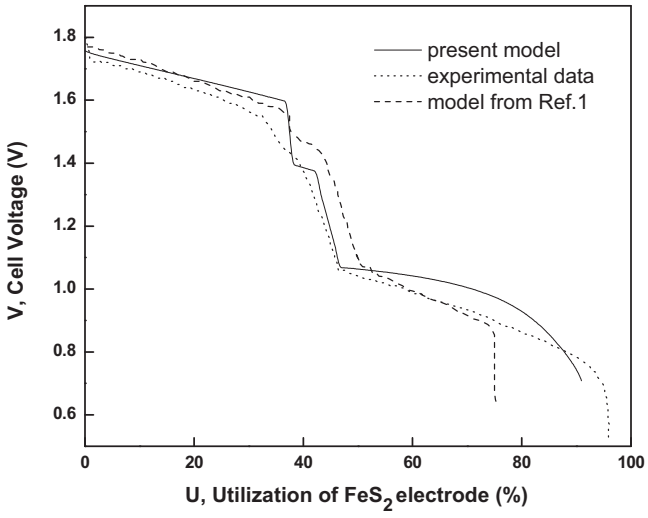

Fig. 4. Comparison of simulated discharge profile with experimental data and model results in literature (I_{app} = 50 mA cm^{-2}).

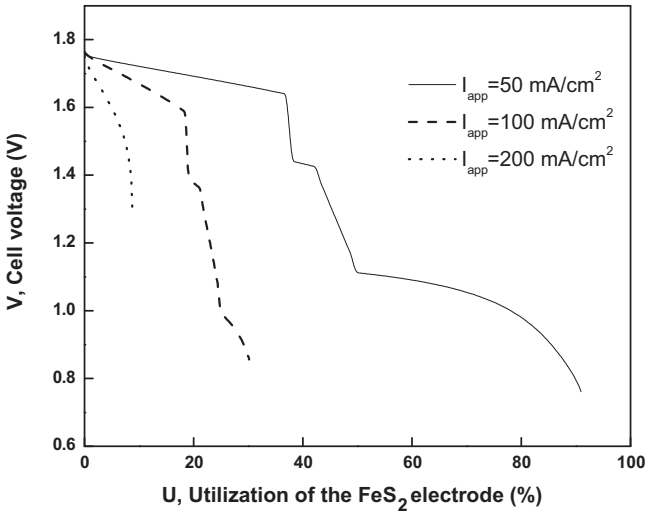

Fig. 5. Model results of the cell voltage at different current densities.

firstly because the producing amount of Li_2S is two times of Fe due to the stoichiometric coefficient of reaction (R2d), secondly because the molar volume of Li_2S is much larger than the mole volume of Fe.

4.3. Discharge behavior

Fig. 4 shows the cell voltage profile for galvanostatic discharge, as a function of the utilization of the FeS_2 electrode. As shown in Fig. 4, it is apparent to distinguish the cell voltage profile consists of four regions. The four regions correspond to the four-stage discharge reactions sequence. Fig. 4 also shows the comparison of the discharge curves between the present model results, the model results from Ref. [1] and the experimental data from Ref. [14]. The value of S = 0.5 was used to simulate the discharge profile for a lithium rich electrolyte (68% LiCl) at 450 °C with a discharge current density of 50 mA cm^{-2}. The same simulation parameters were applied to the experimental data and Bernardi's model. The discharge profile obtained from the model presented in Ref. [1] did not consider dimension change in the positive electrode. The model without considering the volume expansion under-predicts the capacity of the battery severely (20%). It is therefore demonstrated that the inclusion of volume expansion predicting the discharge profile is more accurately. This is because that in the experimental battery system, changes in volume of the reactants lead to plugging of the pores as well as expanding/contracting the electrode. The relationship between the expansion velocity and the porosity is established in the present study. This has resulted in an increase in the utilization of the electrode and thus agreed the capacity of the battery better with the experimental data compared to the model in Ref. [1].

Fig. 5 illustrates the effect of increasing discharge current density on the discharge behavior. It is apparently observed that the active material utilization is limited at higher discharge rates. At the 100 mA cm^{-2} discharge current density, the cell potential drops sharply when about 35% of the cathode material is utilized, this is because the overpotential induced by the higher discharge current density increases, in turn, the domination of the reactions (R2b) and (R2c) are initiated sooner than for the case with a lower current density (e.g., 50 mA cm^{-2}). For an even higher discharge current density, for instant, 200 mA cm^{-2}, we even could not observe the four-region discharge behavior because the discharge current density is so high that hinder the utilization of the active material. In this case, before the reaction (R2b) predominated, the cell voltage has dropped to the cell cutoff voltage. From Fig. 5, we found that the higher the current density is, the faster the voltage cell drops to reach the cell cutoff voltage 1 V.

4.4. Temperature behavior

As we discussed above, the temperature coefficient b_i (shown in Table 1) of individual reaction in cathode can give us an indication of the temperature behavior of a cell during the discharge process. When the temperature coefficient b_i is positive, it means the reaction is endothermic; consequently, the temperature would decrease. In contrast, when b_i is negative, the counterpart temperature would increase. Fig. 6 shows the temperature change on the interface between the cathode and the current collector as a function of discharge time. It is observed that the temperature decreases sharply before the utilization reaching 42%, this is because before the utilization approaching 42%, reaction (R2a) with a positive temperature coefficient (0.475×10^{-3} V K^{-1}) predominates in the discharge reactions sequence and the rest three reactions play slight roles in the change of cell temperature.

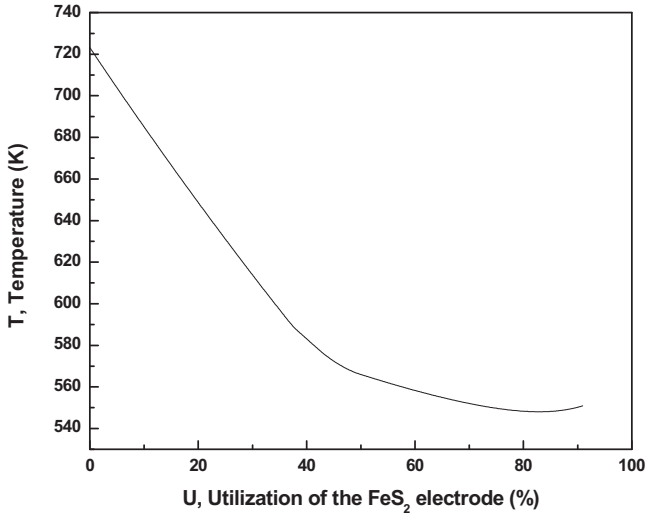

Fig. 6. The temperature on the interface between the cathode and the current collector as a function of discharge time.

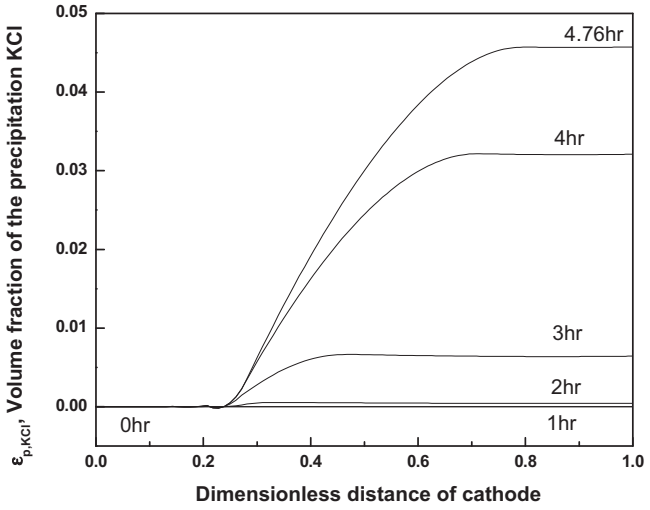

Fig. 7. Volume fraction distribution of precipitation KCl in the positive electrode for various discharge times with $k_p = 0.001\ \mathrm{cm^3\ mol^{-1}\ s^{-1}}$.

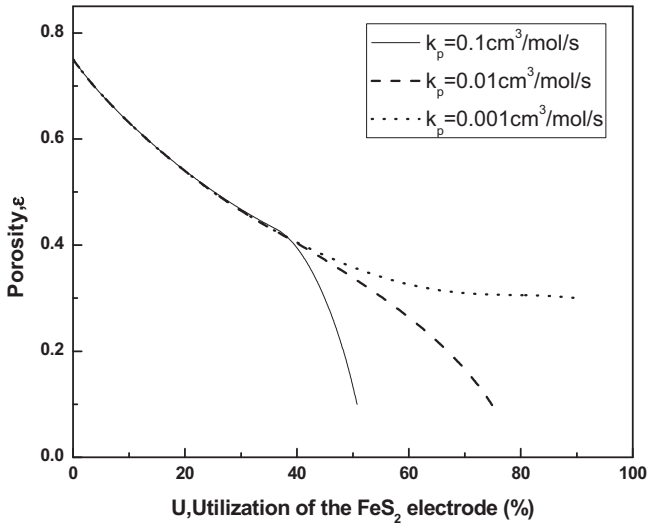

Fig. 8. Change in porosity on the interface between the cathode and the current collector as a function of utilization of FeS_2 for different KCl precipitation rate constants.

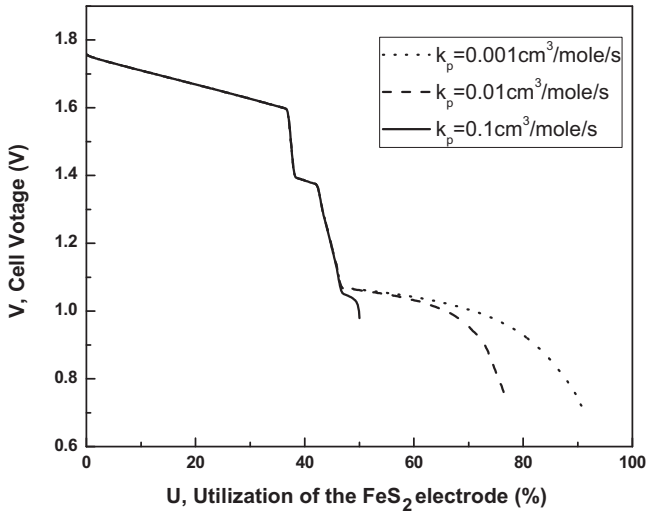

Fig. 9. Voltage change with utilization of the FeS_2 electrode at a discharge current density of $50\ \mathrm{mA\ cm^{-2}}$ for different KCl precipitation rate constants.

When the utilization proceeds, reaction (R2a) has reached its completion, instead reactions (R2b)–(R2d) contribute a lot to the temperature change. In this region, the temperature declines mildly firstly because of the negative temperature coefficient of reaction (R2d) ($-0.147\ \mathrm{V\ K^{-1}}$), secondly because the precipitation of KCl occurs and the polarization heat becomes increasingly important. At the end of the discharge process, one reason why the temperature increases a little rather than continuously decreasing is that reaction (R2d) becomes the dominating reaction and it is exothermic. Another reason responding for the phenomena is still the polarization heat due to the KCl precipitation.

4.5. Effect of precipitation of salt KCl on the cell behavior

In the anode, lithium ions produced in reaction (R3) may react with chloride ions in the electrolyte to make lithium chloride crystals that precipitate out of the electrolyte to form solid lithium chloride, meanwhile, in the cathode where lithium ions are consumed causing potassium ions exceeded. The excess amount of potassium ions may also react with chloride ions to form solid potassium chloride according to reaction (R4). However, based on the analysis in Ref. [3], the precipitation of LiCl is avoided, so the precipitation of KCl is the emphasis in this work. When the reactions occurred in the positive electrode consume lithium ions, the mole fraction of salt LiCl decreases below the saturation value of $(x_A)_{sat,KCl}$, which results in the onset of KCl precipitation. Fig. 7 shows the distribution of the volume fraction of solid KCl in the positive electrode at different discharge times when the precipitation rate constant, k_p, is $0.001\ \mathrm{cm^3\ mol^{-1}\ s^{-1}}$. During discharge, at the separator–positive electrode interface, the volume fraction of solid KCl is zero. With shifting inward from the separator–positive electrode interface, the volume fraction of solid KCl occurs at about 25% depth of the positive electrode. With discharge time increases, the volume fraction of solid KCl increases.

The precipitation of KCl salt on the electrode partially blocks the interface between the electrode and electrolyte, in turn reduces the electrochemical active surface, consequently, and causes the change in porosity. In addition, the variation of porosity in the electrode is due to the electrochemical reactions and the parasitic side reaction. In the positive electrode the side reaction resulting in the occurrence of KCl precipitation also leads to the change in porosity. Fig. 8 presents the precipitation effect on the change in the porosity at the interface between the cathode and the current collector as a function of utilization of FeS_2 electrode. The porosity at the interface between the cathode and the current collector decreases with the utilization of the FeS_2 electrode increases, and the decrease along with the utilization of the FeS_2 electrode in the porosity with a large k_p is sharper than that with a small k_p. As shown in Fig. 8, the porosity does not change much at the end of the discharge process (about 90% utilization of FeS_2 electrode), when $k_p = 0.001\ \mathrm{cm^3\ mol^{-1}\ s^{-1}}$. However, when k_p increases to $0.1\ \mathrm{cm^3\ mol^{-1}\ s^{-1}}$, the porosity decreases sharply at 50% utilization of the FeS_2 electrode, which may limit the discharge capacity.

To elucidate the effect of k_p on battery performance, the change in cell voltage along with the utilization of the FeS_2 electrode for different values of k_p is presented in Fig. 9. The discharge capacity increases with decreasing k_p. From the discharge curve, we can distinguish the four regions clearly, which supports the four-region behavior of the FeS_2 electrode. However, with larger value of k_p (e.g. $0.1\ \mathrm{cm^3\ mol^{-1}\ s^{-1}}$), the porous electrode becomes plugged as shown in Fig. 8, so that the discharge process of the FeS_2 electrode is incomplete. In order to avoid this situation, the precipitation of KCl should be decreased by increasing the temperature, the LiCl

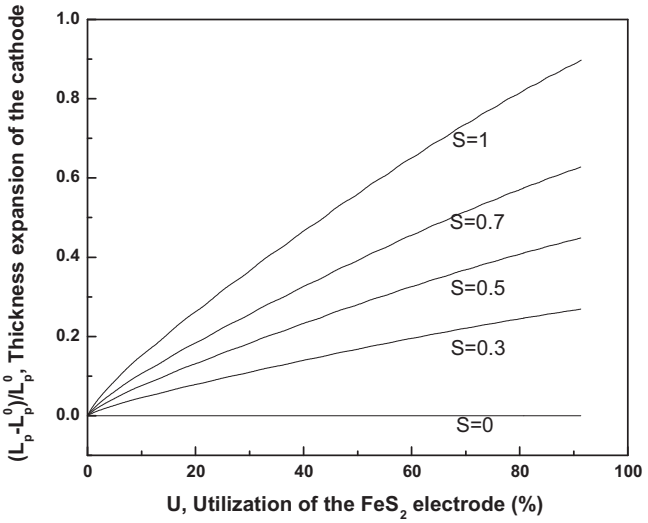

Fig. 10. Expansion of cathode as a function of cathode utilization for different values of swelling coefficient *S*.

concentration in the electrolyte, the porosity of the electrode and so on.

4.6. Dimension change in the positive electrode

The change in dimension of the positive electrode during the discharge process is shown in Fig. 10 for various values of swelling coefficients. It can be observed from the profile that the amount of volume expansion increased with an increase in the value of *S*. When $S = 0$, where all of the volume change results in changing in the porosity, the dimension of the electrode does not change, which is the situation Bernardi's model considered. After extending Bernardi's model by including the local electrode displacement velocity, the trend of the dimension change in the cathode is seen clearly: As *S* increases, the thickness expansion of the electrode keeps increasing with the utilization of FeS_2 electrode.

5. Conclusions

A mathematical model for a LiAl/LiCl–KCl/FeS_2 cell has been developed which can be used to predict the variation of the concentration of the ionic species in the melt and the volume fractions profiles of individual solid species as a function of time and space. Discharge behavior, the high discharge current density effect and cell temperature behavior are also investigated. Moreover, our model predicts that KCl precipitation can limit the utilization of the FeS_2 electrode and discharge capacities. To enhance the capacity, the precipitation of KCl should be decreased by increasing the cell temperature, the LiCl concentration in the electrolyte, and the porosity of the electrode. Furthermore, our model is also developed to account for the volume change in high temperature battery system. The volume change in the cathode during discharge is attributed to the change in porosity and the change in the dimension of the electrode. Based on the material balance, the relationship between the porosity and the local electrode displacement velocity is presented. It was found that inclusion of the change in dimension of the electrode is vital for accurate prediction of the discharge curve. The model agrees well with the experimental data and could be used to optimize the design parameters for other operating conditions of lithium–aluminum, iron disulfide high temperature battery system.

Acknowledgement

The authors are grateful for the financial support for this project provided by the National Reconnaissance Office (NRO) under contract # NRO-000-03-C-0122.

Appendix A.

The physical properties of the electrolyte are given below based on Refs. [3,6].

The effective conductivity of the electrolyte is given by the following expression:

$$K^{eff}\ \ (\Omega\,\mathrm{cm}^{-1}) = \varepsilon^{1.5}(18.9803x_A^2 - 5.0170x_A + 9.0903)\exp\left(\frac{-1425.76}{T}\right) \tag{A.1}$$

The chemical potential gradient of salt A is given by:

$$\nabla\mu_A\ \ (\mathrm{J\ mol}^{-1}\,\mathrm{cm}^{-1}) = RT\left(1 + \frac{d\ln\gamma_A}{d\ln x_A}\right)\nabla\ln x_A \tag{A.2}$$

where the activity coefficient is given by the following expression:

$$\ln\ \gamma_A = \frac{-1555.11}{T}\tanh\left(\frac{1023.84(1-x_A)^3}{1555.11x_A}\right) \tag{A.3}$$

The effective diffusion coefficient of lithium ions in the electrolyte is given by:

$$D^{eff}\ \ (\mathrm{cm}^2\,\mathrm{s}^{-1}) = 2.442\times10^{-4}\exp\left(\frac{-1425.76}{T}\right)(x_A + 0.4)\varepsilon^{0.5} \tag{A.4}$$

Applying Maxwell's model, we assume that the solid phase consists of a continuous phase and several discrete phases. In our system, Fe and voids are assumed to be the discrete phases and other electrode phases are lumped together and called the continuous phase. Consequently, the solid effective conductivity is given by:

$$\frac{(\sigma^{eff}/\sigma_c) - 1}{2((\sigma^{eff}/\sigma_c) + 1)} = \left(\frac{(\sigma^{eff}/\sigma_c) - 1}{2((\sigma^{eff}/\sigma_c)) + 1}\right)\varepsilon_{\mathrm{Fe}} - \varepsilon \tag{A.5}$$

where σ_c is the conductivity of the continuous phase

$$\sigma_c = \frac{\varepsilon_{\text{Z-phase}}\sigma_{\text{Z-phase}} + \varepsilon_{\text{X-phase}}\sigma_{\text{X-phase}} + \varepsilon_{\mathrm{Li_2S}} + \sigma_{\mathrm{Li_2S}} + \varepsilon_{\mathrm{FeS_2}}\sigma_{\mathrm{FeS_2}}}{\varepsilon_{\text{Z-phase}} + \varepsilon_{\text{X-phase}} + \varepsilon_{\mathrm{Li_2S}} + \varepsilon_{\mathrm{FeS_2}}} \tag{A.6}$$

The molar volume of the electrolyte is defined as the following expression:

$$\tilde{V}_e = \frac{(74.555 - 32.161\times x_A)\times10^{-16}}{(2.16233194 - 0.00073684) - 0.15\times(x_A - 0.00147368\times T - 0.36253409)} \tag{A.7}$$

The equilibrium composition that characterized the onset of precipitation of KCl is approximated by:

$$(x_A)_{\mathrm{KCl},sat} = 0.14615 + 1.9117\times10^{-3}T - 1.948\times10^{-6}T^2 \tag{A.8}$$

References

[1] D. Bernardi, J. Newman, J. Electrochem. Soc. 134 (1987) 1309–1318.
[2] R.A. Guidotti, Paper presented at the 27th International SAMPE Technical Conference, Albuquerque, New Mexico, October 9–12, 1995.
[3] R. Pollard, J. Newman, J. Electrochem. Soc. 128 (1981) 491–502.
[4] R. Pollard, J. Newman, J. Electrochem. Soc. 126 (1979) 1713–1717.
[5] R. Pollard, Ph.D. Dissertation, University of California, Berkeley, 1979.
[6] D.M. Bernardi, Ph.D. Dissertation, University of California, Berkeley, 1986.
[7] Z. Tomczuk, B. Tani, N.C. Otto, M.F. Roche, D.R. Vissers, J. Electrochem. Soc. 129 (1982) 925–931.
[8] R.A. Guidotti, P. Masset, J. Power Sources 177 (2008) 595.
[9] P. Butler, J. Power Sources 139 (2004) 240.

[10] R.A. Guidotti, P. Masset, J. Power Sources 161 (2006) 1443.
[11] M. Au, J. Power Sources 115 (2003) 360.
[12] R.A. Guidotti, F.W. Reinhardt, Proceedings of the 17th Conference on Application and Advances, 2001.
[13] D.E. Reisner, T.D. Xiao, J. New Mater. Electrochem. Syst. 2 (1999) 279.
[14] G. Sikha, B.N. Popov, R.E. White, J. Electrochem. Soc. 151 (2004) A1104–A1114.
[15] M.K. Jain, G. Nagasubramanian, R.G. Jungst, J.W. Weidner, J. Electrochem. Soc. 146 (1999) 4023–4030.
[16] J.S. Dunning, Argonne National Laboratory Report ANL-80-128, 1981, p. 190.
[17] M. Sudon, Newman, J. Electrochem. Soc. 137 (1990) 876–883.
[18] P.M. Gomadam, J.W. Weidner, J. Electrochem. Soc. 153 (2006) A179–A186.
[19] COMSOL Multiphysics Simulation Package, see at: http://www.it.comsol.com.